RFID-Based Sensors for Zero-Power Autonomous Wireless Sensor Networks

Benjamin S. Cook, *Student Member, IEEE*, Rushi Vyas, *Student Member, IEEE*,
Sangkil Kim, *Student Member, IEEE*, Trang Thai, Taoran Le, Anya Traille,
Herve Aubert, *Senior Member, IEEE*, and Manos M. Tentzeris, *Fellow, IEEE*

Abstract—Radio frequency identification (RFID) technology has enabled a new class of low cost, wireless zero-power sensors, which open up applications in highly pervasive and distributed RFID-enabled sensing, which were previously not feasible with wired or battery powered wireless sensor nodes. This paper provides a review of RFID sensing techniques utilizing chip-based and chipless RFID principles, and presents a variety of implementations of RFID-based sensors, which can be used to detect strain, temperature, water quality, touch, and gas.

Index Terms—Wireless sensors, RFID, inkjet printing, mm-wave.

I. INTRODUCTION

WIRELESS sensor networks have rapidly become an integral part of our everyday lives. Whether they are monitoring suspension bridges that experience immense forces from storms and earthquakes for structural integrity [1]–[4], detecting noxious gases in underground mines [5]–[7] or ensuring that the vegetables on the supermarket shelf are still fresh and being kept at the correct temperature and humidity level [8]–[10], sensor networks are giving us the ability to compile massive amounts of data which can greatly improve our knowledge of the environment around us. To enable large-scale pervasive sensor networks which collect this data, the sensing platform has to be reliable, energy efficient, and extremely low cost to become a viable long-term solution

Previous methods for deploying large-scale sensor networks involved running long lengths of cabling which would source power and collect data from each individual sensor, or the installation of battery-powered wireless transceiver-integrated sensors which remove the need for cabling, but in turn pose a long-term environmental risk with the disposal of billions

of batteries [11], [12]. While these methods were necessary in some situations where real-time data was required or harsh environments prohibited manual monitoring of critical environment data, the cost, installation difficulty, and maintenance rarely justified their use over manual data collection.

This is where the concept of "zero-power" radio frequency identification (RFID) tag-based sensors comes in. The first RFID tags were introduced in the early 1970's to enable the passive identification and tracking of inventory for supply chain management, access control, and real-time location systems (RTLS) [13]. The tags were designed to be low-cost and robust to allow for the identification and tracking of everything from envelopes and shipping containers to employees entering and leaving restricted access areas. RFID tags are typically passive in nature and work on the principle of wireless backscatter modulation to transmit data without the requirement for a power source on the tag. Each RFID tag has a unique identifier or signature which is encoded onto the backscatter of the interrogation signal from a RFID reader. Utilizing this passive backscatter-based encoding technique, a single powered reader can retrieve individualized data from large quantities of densely packed mobile tags from a centralized location.

This RFID platform which was originally developed for large-scale asset tracking happens to be an excellent backbone for building low-cost large-scale wireless sensor networks. The platform has several key characteristics including being wireless, passive, low-cost, and low maintenance which make deploying massive amounts of sensors practical. Meanwhile, as the RFID platform is already widely accepted throughout industry, large-scale sensor networks based on RFID technology can be seamlessly integrated into current off-the-shelf RFID systems. These factors give RFID-based sensor networks the potential to become the ultimate sensing tool to collect and compile massive amounts of detailed real-time data about the environment around us, potentially enabling a plethora of applications in the areas of Internet of Things, Smart Skins, Man-to-Machine and cognitive intelligence.

The following sections present an overview of RFID sensing principles and techniques, examples of "zero-power" RFID sensors utilizing the aforementioned RFID sensing principles which sense quantities such as strain, temperature, gas, and touch, and a look into state-of-the art energy harvesting techniques which will enable a new class of RFID-based sensors with extended features including data processing and environmental interaction.
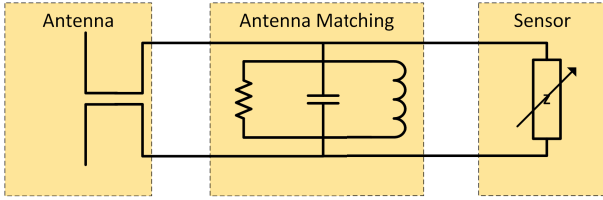
Fig. 1. RFID sensor node exploiting frequency domain "antenna mode" scattering.

II. RFID SENSING SYSTEM TOPOLOGIES

A. Chipless RFID Sensors

RFID-based sensors come in numerous topologies with varying degrees of complexity, the simplest of which requires no integrated circuits (ICs) and transmits sensor data by changing the radar cross section of the RFID tag. The simplified chipless RFID sensor, or scatterer, in Fig. 1 consists of an antenna which operates in the RFID band of interest with an impedance of Z_A, a typical single-band matching network or in some cases a multi-band matching network, and a passive sensor with an impedance Z_L. The sensor, which could be designed for the sensing of gas, strain, temperature, or a variety of other quantities, transforms the physical quantity being measured into a change in electrical properties. This electrical change could be a change in resistance, reactance, charge carrier density, or a variation in the relative permittivity ϵ_r or permeability μ_r. Due to its changing electrical properties, the sensor can be modeled as a variable loading impedance to the antenna which changes proportionally to variations in the measured physical quantity. This change in sensor impedance in turn modifies the matching with the antenna and causes a change in the radar cross section (RCS) of the antenna.

The radar cross section (RCS) of the RFID antenna can be broken down into a linear combination of the complex valued "structural mode" σ_S, and "antenna mode" σ_A scattering [14], [15]. The "structural mode" scattering is dependent on the physical size and orientation of the antenna, and remains constant while the sensor is stationary. The "antenna mode" scattering is dependent on the re-radiated power caused by load mismatch within the antenna and varies with a load impedance variation. The RCS of the RFID in Fig. 1 can be described by Eqs. (1), and (2) where σ is the combined RCS of the "structural mode" and "antenna mode" backscatter, $\vec{E}_i$ is the incident field, $\vec{E}_r$ is the reflected field, Γ is the reflection coefficient between the antenna and the input impedance of sensor which contributes to the "antenna mode" backscatter, and A_s is a constant which contributes to the "structural mode" backscatter [16]."

$$\sigma = \lim_{r \to +\infty} 4\pi r^2 \frac{|\vec{E}_r|^2}{|\vec{E}_i|^2} = \frac{\lambda^2}{4\pi} G^2 |\Gamma - A_s|^2 \quad (1)$$

$$\Gamma = \frac{Z_{in} - Z_a^*}{Z_{in} + Z_a} \quad (2)$$

When the antenna and load impedance Z_A and Z_{in} are matched, the antenna mode reflection, Γ, goes to zero, meaning there is no "antenna mode" component to the backscattered
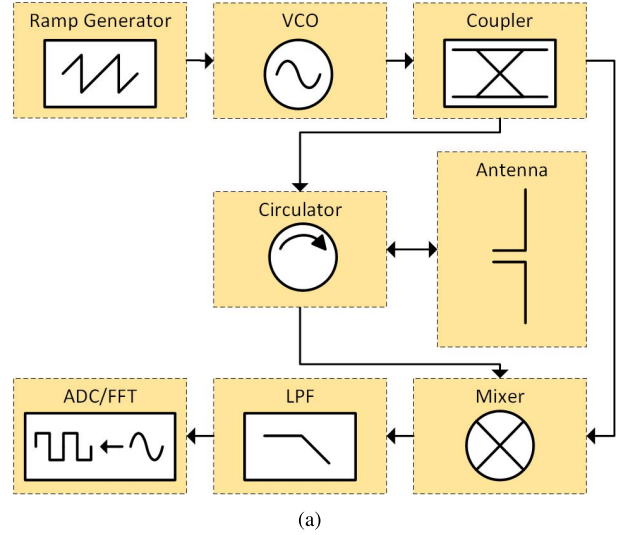

(a)

(b)

Fig. 2. (a) Block diagram of a typical FMCW reader and (b) an interrogation, and backscattered up-chirp signal.

signal contributing the RCS, σ. As the mismatch increases with a change in sensor impedance, the "antenna mode" backscattered signal, Γ, will also increase. As the "structural-mode" component of the RCS remains constant, the change in the RCS is directly related to a change in the "antenna-mode" component. The change in RCS can then be translated back to a change in a physical quantity sensed by the sensor utilizing pre-determined calibration coefficients. It is important to note that the RCS of the antenna is frequency dependent, as is the sensor impedance, which allows for detecting distinct frequency dependent RCS signatures to enhance sensing accuracy.

A typical frequency modulated continuous wave (FMCW) reader used to measure the RCS of an RFID sensor node is displayed in Fig. 2(a).

The FMCW reader works by sending a ramp modulated, or up-chirp wave to the sensor which linearly increases the frequency from f_{start} to f_{stop}. This up-chirp signal repeats with a sweep time T_S. The received backscatter, which is time-delayed, is mixed down with the up-chirp signal. The difference in frequency due to propagation delay produces a beat frequency f_b which is determined by Eq. (4) where B_{sweep} is the bandwidth of the up-chirp signal sweep, R is the radial distance of the RFID sensor node, and c is the speed of
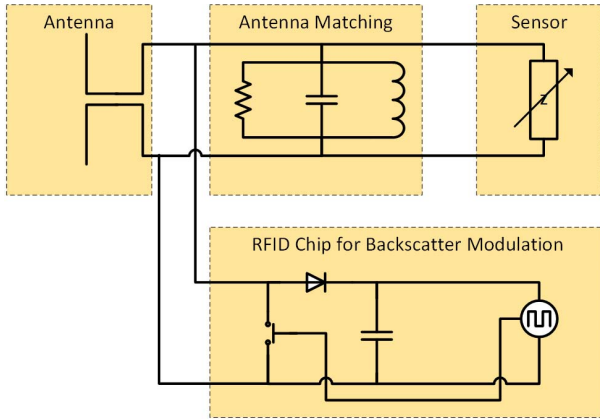
Fig. 3.   RFID sensor exploiting digital backscatter modulation.

light in free space [17], [18].

$$B_{sweep} = f_{stop} - f_{start} \qquad (3)$$

$$f_b = \frac{B_{sweep}}{T_S} \frac{2R}{c} \qquad (4)$$

Utilizing the amplitude and beat frequency of the backscattered signal, the distance to the sensor, and the radar cross section of sensor can be determined. While this method is by far the simplest and lowest cost method of implementing RFID-based wireless sensors, it is more vulnerable to multipath and environmental effects as digital modulation schemes are not employed on the sensor end to remove the scattering effects of surrounding environment ("ambient") objects and an initial calibration must be performed to remove these effects. However, if this method is used in an un-cluttered environment such as on the external walls of a large building, multipath effects are much less prevalent and the simplicity of the system results in a very low cost solution. Several methods can be used to reduce multi-pathing and environmental effects including incorporating multiple resonators to produce multiple reference points in the frequency domain [19], delay lines to allow for time-gating of environmental backscatter [20], [21] , and diode frequency doubling to introduce frequency domain removal of environmental backscatter [22], [23]. Chipless RFID sensors have been demonstrated with read ranges of several meters [8] up to 30 m [24].

B. Chip-Based RFID Sensors

In situations where there are rapidly changing environmental conditions, or a large number of sensors in close proximity, a better method of identifying individual tags than RCS-based backscatting is required. To solve this problem, digital modulation is incorporated into the backscattering approach as it allows for the unique identification of a large number of tags, anti-collision protocols, and data transmission which are all part of the RFID EPC-Gen2 protocol [25]. To incorporate digital modulation into the backscattered signal, an RFID chip is added to the tag as shown in Fig. 3.

1) Chip-Based Topology 1: Similar to the RCS-based detection of the chipless tags, the sensor changes the frequency-dependent RCS of the "antenna mode" backscatter due to the
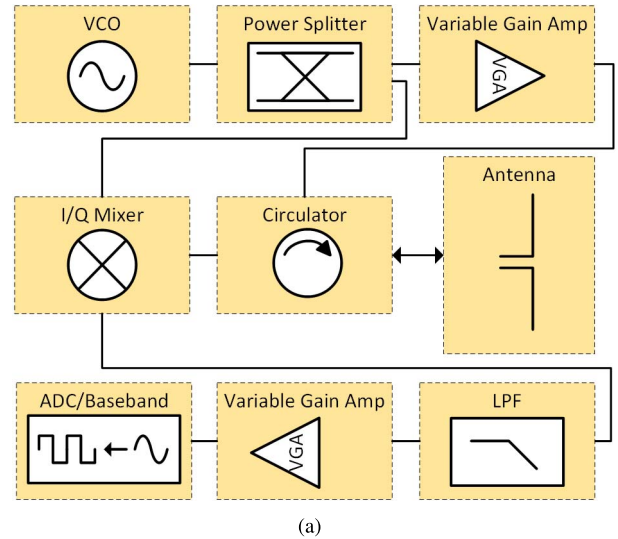

(a)

(b)

Fig. 4.   (a) A block diagram of a simple RFID reader for reading EPC-Gen2 RFID tags and (b) ASK modulation backscattering from an RFID tag.

load impedance mismatch. To digitally modulate the backscatter, the RFID chip rectifies energy from the interrogation signal using an RF to DC converter and stores the energy in a capacitor. The chip is matched to the antenna impedance in its initial state to ensure maximum power transfer into the rectifier, which in turn minimizes the "antenna mode" RCS. When the voltage in the capacitor reaches the threshold level, the IC wakes up and sends a digital waveform to a switch within the chip which in turn presents a changing impedance to its terminals causing the RCS of the RFID sensor to vary in amplitude and/or phase, also known as amplitude-shift keying (ASK) or phase-shift keying (PSK) [26], [27]. In this case, ASK and PSK are time-domain modulation schemes which are used to encode the sensor ID. On top of the modulation from the chip, the sensor still presents a frequency-dependent load to the antenna which varies the amplitude of the modulated signal over frequency. This creates a second-tier frequency domain modulation of the signal. Utilizing the time and frequency modulated signals from the tag, both the identity of the tag, and the sensor information can be extracted.

The reader, which is shown in Fig. 4(a), is slightly more complicated than the FMCW reader as it needs to be able to demodulate the frequency and time coded digital backscatter modulation. Instead of sending a chirped continuous
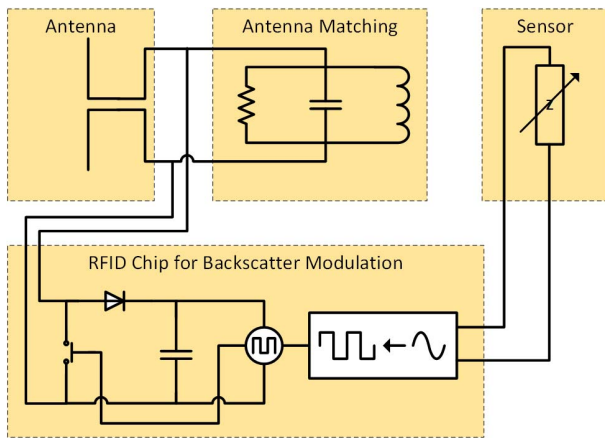
Fig. 5. RFID sensor node which incorporates sensor data into a data packet along with the chip ID.

Fig. 6. RF spectrum measured in Tokyo, Japan.

Fig. 7. RFID sensor node self-powered by harvesting ambient RF energy.

wave (CW) signal, the reader for the IC-based tags generates a single frequency CW signal. The backscattered power is decomposed into its I and Q components and then digitized and processed in the baseband [28]. To recover the frequency dependent RCS due to the sensor, the CW oscillator frequency is swept through several discrete frequency points within the RFID band [29]. This is a much more robust solution when it comes to deploying large amounts of sensors as sensor identification and anti-collision become possible, and because of this, is the currently most common RFID sensor topology. Passive chip-based RFID sensors have been shown to operate at ranges up to 3–5 m while transmitting within FCC limits [29]–[31].

2) Chip-Based Topology 2: A second chip-based RFID sensor topology, which has recently been gaining popularity due to its robust nature, incorporates the sensor data directly into the digital modulation of the backscatter as shown in Fig. 5. To do so, the sensor output values are converted to a DC or low-frequency AC voltage using a resistor divider circuit, and is measured by an analog-to-digital converter (ADC) which is incorporated into the RFID chip. The digitized sensor data is then encoded into a packet with the chip ID and modulated onto the backscatter signal. While this topology allows for more precise sensor measurements, it is significantly more expensive, and the read range suffers as more power is required for computation and digitization of the sensor data.

C. Autonomous Energy Scavenging RFID Sensors

The previously discussed RFID sensor topologies are excellent candidates for low-cost, short-range, and high-density sensing networks. However, due to the nature of backscatter-based tags, the read range is limited by the power emitted from the reader. In situations where long-range sensing over 10–20 meters is required, the high path losses decrease the power of the backscattered signal below the noise floor of the RFID reader. Initially, the solution was to make the tags active, meaning a power source needed to be attached to the tag to boost the tag turn-on sensitivity and backscattered power level. However, this detracts from the initial motivation of RFID
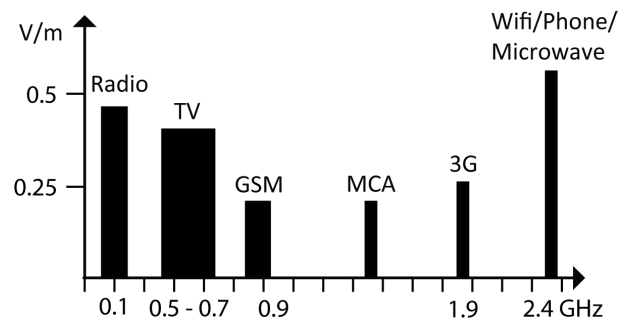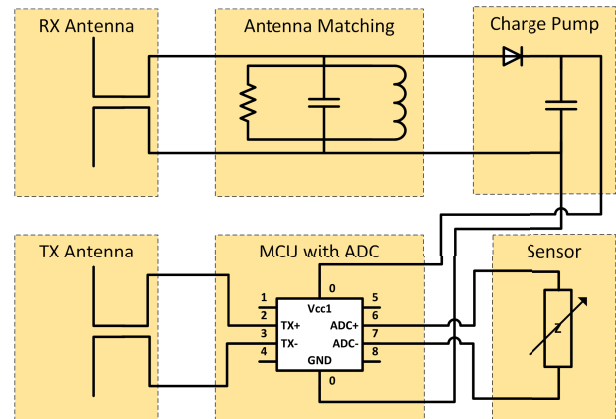
sensors which was to remove the requirement for batteries or power sources on the sensor nodes themselves.

To address this problem, recent work has been focused on incorporating wireless energy scavenging into the chip-based RFID sensor topology [32]–[34]. The air is full of ambient RF signals from TV stations, WiFi networks, radio stations, cell towers, and appliances. And, unlike solar and vibrational energy sources, ambient RF is being emitted constantly and can be harvested indoors and outdoors. An approximate spectrum of ambient RF energy in a metropolitan area is shown in Fig. 6.

The energy scavenging RFID sensor in Fig. 7 has a wide-band RX antenna which is tuned to capture RF signals in the digital TV, WiFi, and cellular bands. This energy is converted to DC in an RF-DC converter, or charge pump, which is then stored in a capacitor. A microcontroller (MCU) with a power management unit (PMU) awakes when it senses the capacitor voltage is above the threshold voltage, reads and records the sensor value, and transmits the data via an on-board transmitter using the RFID communication protocol. When the PMU detects that the voltage on the capacitor is too low, it puts the MCU back to sleep and waits for the capacitor to re-charge. The duty cycle at which the RFID sensor can read the sensor and transmit data depends on the amount of ambient RF energy. In dense urban areas, the RFID sensor can transmit the sensor data to remote receiver nodes/gateways several times per minute, while in sparsely populated rural areas, it may only be able to transmit once every several minutes.

TABLE I
COMPARISON OF RFID SENSING TOPOLOGIES

	ID	Modulation	Range (m)	Cost ($)
Chipless	Analog	Freq. Signature	30	0.05-0.2 [24]
Chip Type 1	Digital	Freq. Signature	5-10	0.2-0.5 [35]
Chip Type 2	Digital	ASK	4.5	0.5-2 [36]
Autonomous	Digital	ASK	6300	2-10 [32]

Current works show state-of-the-art energy harvesting sensors working up to 6.3 km away from the nearest digital television towers [32], [33].

D. RFID Sensor Topology Summary

A summary of the discussed sensor topologies is presented in Table I. The sensors are compared against their identification method, sensor modulation technique, average communication range, and approximate cost. Each topology comes with its own strengths and weaknesses. For low-cost monitoring in uncluttered environments, such as temperature monitoring on the walls of a building, RCS-based backscatter sensors are an excellent solution. However, in situations where monitoring at long-ranges is required, sensors which can harvest their own energy and transmit the data to remote receivers is a better option.

III. RFID SENSOR IMPLEMENTATION

The theoretical discussion of the four typical RFID sensor topologies presented earlier forms the foundation for understanding how "zero-power" wireless sensor networks sense and communicate. However, there are a vast array of methods used to implement these sensor topologies for real-world sensing applications. Practical implementation of each of the four sensor topologies will be discussed in the following sections along with various methods to interface sensors for gases, fluids, temperature, touch, and strain.

A. Chipless RFID Strain Sensors

Current engineering structures are susceptible to cyclic loading and harsh environments which cause deterioration and stress fractures over the structures lifetime. To remain in service for long periods of time, these structures require constant inspections to detect and prevent potential structural problems. Failures or down time due to required inspections present significant costs in time and resources. Periodic manual inspections, which are primarily visual, are difficult and nearly impossible in some situations where there are hard to access areas or cracks underneath the paint. The first chipless RFID sensor presented in this article is a strain sensor proposed by Thai et al. for monitoring strain values down to 1 milli-strain on the exteriors of large structures such as bridges and buildings to aid in early detection of structural integrity issues [4]. The sensor shown in Fig. 8 utilizes the first sensing topology which utilizes an FMCW reader to determine changes in the RCS of the sensor.
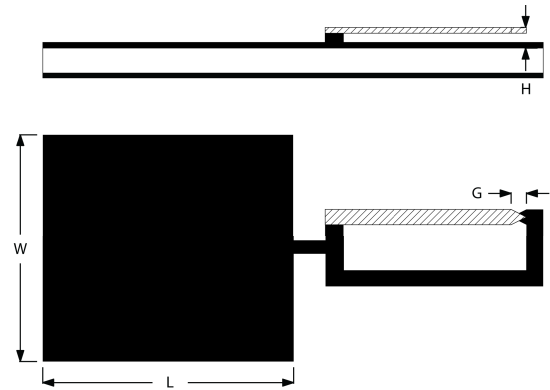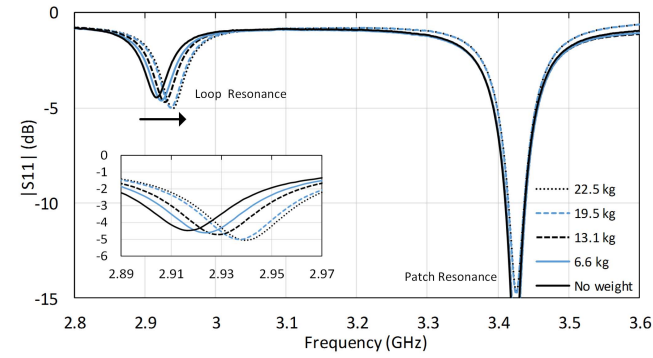

Fig. 8. Design of the strain-sensing chipless RFID sensor.

To create an RCS change which is linear with respect to strain, the patch antenna in Fig. 8 is loaded with a microstrip resonant loop which has a slightly offset resonant frequency from the patch. The resonant loop is an L-C resonator in which the capacitive gap is created by a cantilever which is disconnected from the substrate. This is done to isolate the cantilever from any strains experienced by the substrate. The cantilever is made from a material with low-coefficient of thermal expansion to reduce temperature diffraction of the beam. As sheer force in a direction parallel to the length L of the patch is applied to the substrate, the patch antenna and the portion of the resonant loop affixed to the substrate experience strain, or stretching, while the cantilever maintains its original length. This causes a change in the horizontal gap distance G between the cantilever and loop, which in turn changes the capacitance of the gap. The triangular taper on the end of the cantilever and loop increase the linearity of the resonant frequency versus strain characteristics.
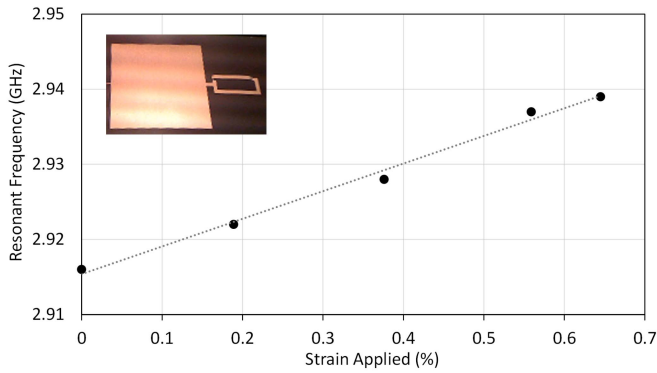
The measured return loss of the chipless strain sensor in Fig. 9(a) shows that the sensor has two resonances–the resonance of the patch at 3.4 GHz, and the resonance of the loop at 2.9 GHz. As strain is increased on the substrate, the resonance of the patch remains constant when strain in the milli-strain range is applied as its change in length is on the orders of parts per million (ppm). However, the capacitive gap of the resonant loop is much more sensitive to these small changes in length as the cantilever is detached from the substrate under strain. As the gap increases due to tensile strain, the capacitance decreases which causes an increase in the resonant frequency of the loop. By applying up to 22.5 kg of force, which equates to 7 milli-strain, the resonant frequency of the loop increases by approximately 22 MHz.

Utilizing an FMCW reader similar to the one in Fig. 4, the frequency-dependent RCS is extracted to determine the resonant frequency of the loop and patch resonances. As the patch resonance remains constant over strain, the frequency separation of the patch and loop resonances can be used to determine the strain level based on the calibration curve in Fig. 9(b).

Several other chipless RFID-based strain sensors have also been reported in the literature which use either the patch mode

(a)

(b)

Fig. 9. (a) Measured return loss of the chipless RFID strain sensor and (b) the resonant frequency of the sensor extracted from the measured RCS of the tag.

Fig. 11. (a) Cross section of the microfluidic channel used for the RFID temperature sensor and (b) an optical micrograph of the fabricated microfluidic temperature sensor.

Fig. 12. Measured return loss and capacitance of the microfluidic gap versus temperature.
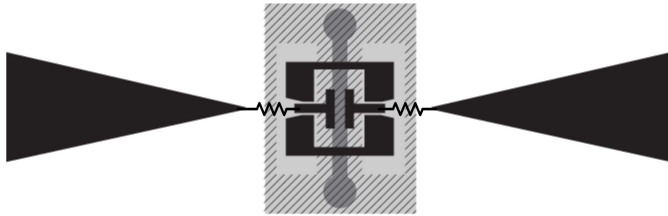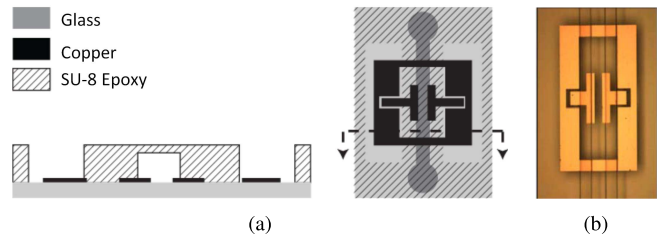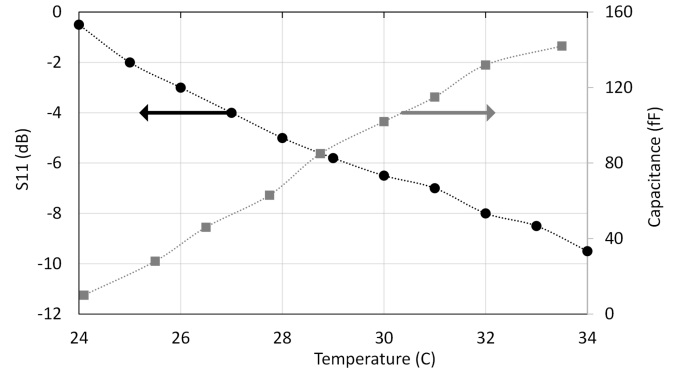

Fig. 10. Design of the chipless RFID temperature sensor.

RCS backscatter [20], [36], [37], or diode doubling of the patch mode RCS to eliminate environmental backscatter noise sources [23].

B. Chipless RFID Temperature Sensors

Temperature sensors are a household item. Nevertheless, they are typically limited to sensing the temperature in a single location. For cooling systems in large buildings, server rooms, and refrigeration trucks, it is critical to understand the temperature gradients with a high spatial resolution to optimize HVAC systems, and ensure machines or food items are being cooled correctly. A chipless based solution by Bouaziz et al. to wireless RFID-based temperature monitoring is shown in Figs. 10 and 11 [8].

To sense the change in temperature, the high coefficient of thermal expansion of water is exploited. Water has the unique property that in the 25 °C–35 °C temperature range, the coefficient of thermal expansion is quasi-linear with an expansion coefficient of approximately 227 ppm/°C. To sense the fluid expansion, a microfluidic channel similar to a thermometer tube is partially filled with water over a planar capacitive gap. As the fluid expands due to an increase in temperature, it covers an increasing amount of the surface of the capacitive gap. As water has a high relative permittivity (ϵ_r) which is approximately 73, the capacitance dramatically increases with increased water coverage.

The capacitor is used as a load in series with a matching resistor for the RFID antenna. At low temperatures, very little water covers the capacitive gap, and the low capacitance presents a high series impedance, or effective open circuit which is highly mismatched with the 50 ohm impedance of the RFID antenna. This mismatch causes a large "antenna mode" backscatter which translates to a large RCS which can be detected by the reader. As the capacitance increases due to increased temperature, the impedance of the capacitance decreases to values closer to an effective short circuit, and the load impedance seen by the antenna is the matching resistor in series with the capacitor. Since the antenna is now better-matched with the load, the "antenna mode" RCS decreases.

The fabricated sensor operates at 29.75 GHz and has dimensions of approximately 1 × 1.5 mm. Measurements of the return loss and gap capacitance of the fluidic capacitor are shown in Fig. 12. As expected, the capacitance increases linearly with temperature. At 24°C the capacitance is approximately 10 fF, while at 34°C the capacitance increases to 130 fF. This 13× increase in capacitance creates a large decrease in the series impedance of the capacitor. This is
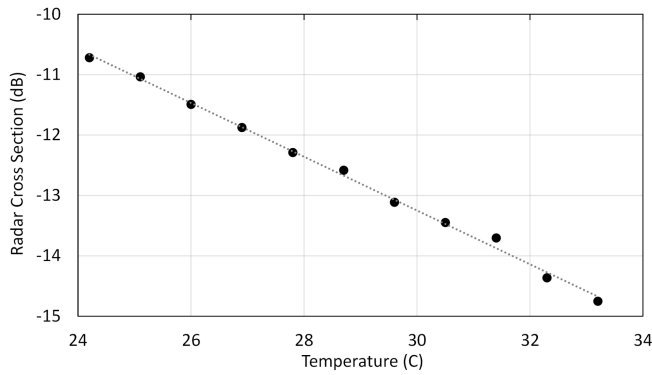
Fig. 13.   Measured RCS of the chipless RFID sensor versus temperature.

(a)

(b)

Fig. 14.   (a) Design of the inkjet printed microfluidic water quality sensor and (b) an optical micrograph of the fabricated sensor.

shown in the return loss measurements. At a low capacitance, the series impedance is high, which causes a high return loss of nearly 0 dB due to load mismatch. However, as the capacitance is increased, the impedance decreases close to that of the series matching resistor, and the return loss decreases below -10 dB.

The measured results from the FMCW reader in Fig. 13 confirm that the RCS decreases with increased temperature. And, since the sensor is operating in the linear expansion region for water and the capacitance is increasing linearly with temperature, the RCS has a highly linear temperature versus RCS curve.

The chipless RFID temperature sensor shows promising results for low-cost temperature monitoring of temperature gradients. Several other chipless temperature sensing implementations have also been investigated in the literature which utilize bimorph cantilever displacement to increase capacitive gaps [38], however, they have a much lower sensitivity than the microfluidic-based sensor presented here.

C. RFID Chip-Based Water Quality Monitoring Sensor

Moving from chipless RFID sensors, chip-based RFID sensors which digitally modulate the backscatter to reduce environmental noise and allow for easier tag identification will be presented. The first chip-based sensor discussed is a microfluidic wireless lab-on-chip (LOC) system initially used for water quality monitoring. Fluid monitoring is a necessary and time intensive task, whether it is for detecting contamination in rivers and lakes, or process monitoring and control in large plants. The microfluidic fluid quality sensor proposed by Cook et al. in Fig. 14(a) utilizes capacitive gap sensing similar to the temperature sensing tag in the previous section, and is fabricated using inkjet printing to greatly reduce the cost [29], [39].

The sensor uses the first chip-based topology in which the sensor information is modulated onto the backscattered power in the frequency domain. However, instead of changing the load impedance of the sensor as a function of sensor state to change the frequency-dependent "antenna-mode" RCS, the resonant frequency of the antenna is changed. Two capacitive gaps are placed in the arms of the dipole-style RFID antenna. When the permittivity of the fluid flowing through the microfluidic channel is low, the two capacitive gaps have
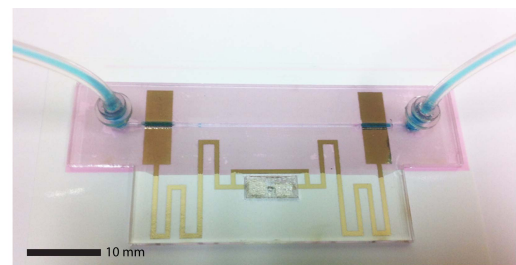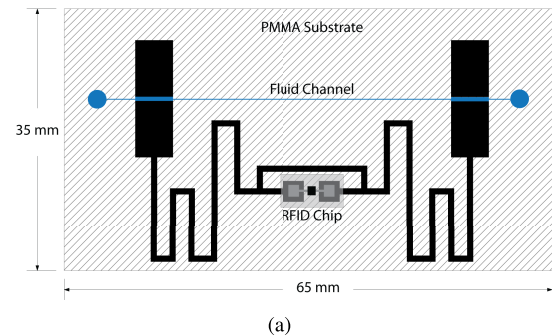
a high impedance, close to that of an RF open. This causes the antenna to look electrically shorter as the currents end at the gap. However, as the permittivity of the fluid in the channel increases, the impedance of the capacitive gap decreases to an RF short which increases the electrical length of the antenna as the currents can easily flow across the gap. The longer the electrical length of the antenna, the lower the resonant frequency. As the impedance of a dipole changes with a resonant frequency change, the matching between the RFID chip and the antenna will change causing a frequency-dependent RCS change which can be picked up by the reader. The chip used in this work is an EPC-Gen2 Higgs-3 RFID chip designed for the U.S. RFID band.

To determine the resonant frequency and impedance of the microfluidic-loaded antenna versus fluid permittivity, cabled measurements of the antenna are performed while several different fluids are fed through the fluidic channels. The fluids include: empty ($\epsilon_r = 0$), hexanol (($\epsilon_r = 3$), ethanol ($\epsilon_r = 15$), water ($\epsilon_r = 73$), and various mixtures of the three. Fig. 15(a) shows the measured return loss of the antenna which has been re-normalized to the chip impedance. When the channels are empty, the resonant frequency is approximately 1000 MHz. By loading the antenna with hexanol, ethanol, and water, the resonant frequency progressively decreases until it reaches 910 MHz when loaded with water only. It can be seen that small changes in permittivity can easily be distinguished due to the large sensitivity. Even sending mixtures of fluid, such as 10 and 20% by weight of ethanol mixed with water can easily be distinguished as shown in Fig. 15(a).

To measure the water quality monitoring sensor wirelessly, a Voyantec Tagformance RFID reader is used, which has a topology similar to that of the theoretical reader in Fig. 4(a). The reader sends a CW signal at one frequency which is increased in power until the reader is able to read the
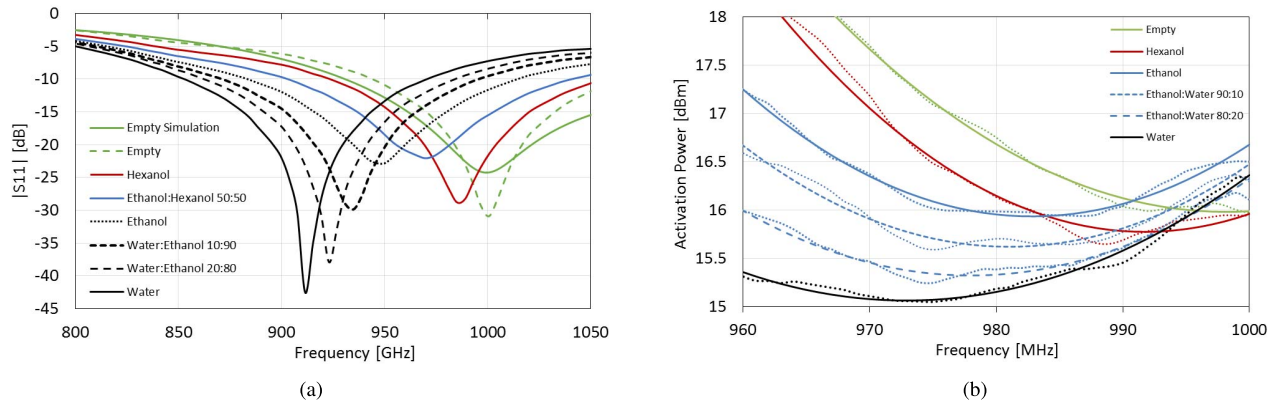
(a)

(b)

Fig. 15.   (a) Measured S-parameters of the microfluidic water quality sensor for various fluids and (b) wireless measurement of the microfluidic water quality sensor.
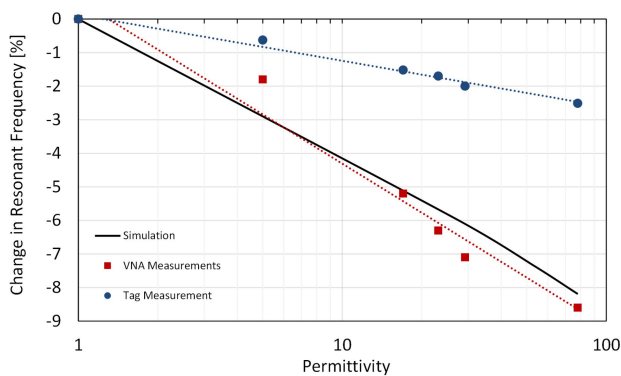

Fig. 16.   Linearity of the microfluidic lab-on-chip system versus fluid permittivity.

tag ID from the backscatter. This is repeated at several frequency points to obtain a frequency-dependent and liquid-mixture dependent scattering model of the antenna to determine its resonance. Again, the tag is measured with an empty channel, and all of the fluids used in the cabled measurement. The data returned from the Tagformance which is shown in Fig. 15(b) displays the transmit power required to activate the tag versus frequency along with the second order curve fit in Matlab which is used to extract the resonant frequency. A clear downward shift in the resonant frequency is experienced as higher permittivity fluids are sent through the channel as is expected.

The linearity of the sensor is displayed in Fig. 16. The linearity of the cabled measurement matches well with the expected log-linear trend of the simulation and has a very high sensitivity to permittivity variations with changes up to nearly 10% in resonant frequency between air and water. The wireless measurement also shows a log-linear trend with changes up to 3% in resonant frequency. As the tag has a frequency-dependent impedance of its own, the wireless measurements have a decreased slightly sensitivity.

The microfluidic LOC is a first-of-its kind microfluidic sensor as it is the first completely passive wireless sensor be able to perform microfluidic measurements. Future work on completely passive LOC RFID systems will enable fluid manipulation as well with the integration of more complex passive RFID chip circuitry.

(a)

(b)
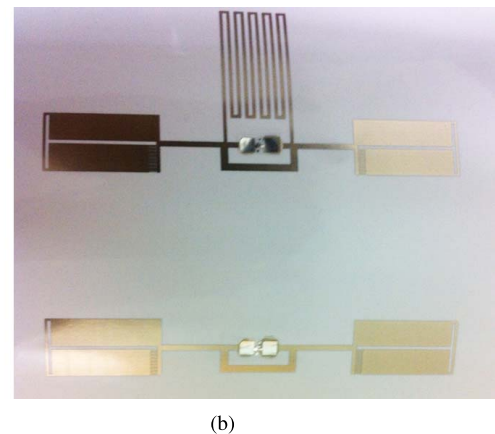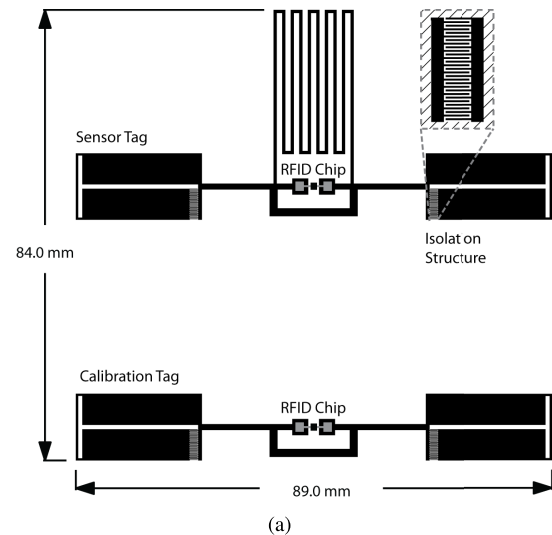
Fig. 17.   (a) Design of the RFID chip-based touch sensor and (b) the inkjet printed RFID touch sensor prototype.

D. RFID Chip-Based Touch Sensor

An inkjet-printed wireless touch and proximity sensor based on the first RFID chip-based sensing topology is proposed by Kim et al. for ultra-low cost touch and proximity sensing [31]. Touch and proximity sensors are becoming popular for applications under the Internet-of-Things (IOT) umbrella to
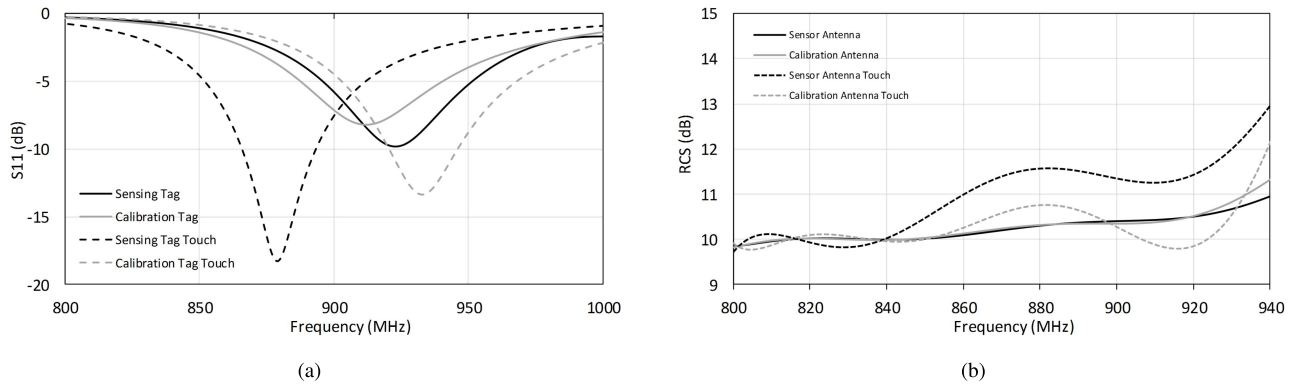
(a)

(b)

Fig. 18. (a) S-parameters of the sensor and calibration antennas with and without a touch event and (b) measured RCS of the RFID touch sensor with and without a touch event.

understand human interactions with objects and environments. The proposed RFID-based touch sensor in Fig. 17(a) consists of the sensing RFID antenna which has a meandered matching network to match the antenna to the EPC-Gen2 Higgs 3 RFID chip, and a calibration RFID antenna which does not perform sensing, but is used as a differential reference for the RFID reader. When a finger, or other object comes in proximity to the meandered matching network of the "sensing" antenna, the matching between the antenna and RFID chip is disturbed which causes a change in the frequency-dependent "antenna mode" RCS of the tag. The RCS of the "calibration" antenna, however, should remain rather constant during a touch event occurring at the sensor antenna due to the isolation structures incorporated into both antennas which minimize crosstalk.

To verify that the matching of the "sensing" antenna is disturbed during a touch event while the "calibration" antenna maintains its original characteristics, the return loss of the two sensors is measured with and without a touch event as shown in Fig. 18(a). The return loss measurements show that both the sensing and calibration antenna have a similar return loss with a resonance near 940 MHz when no objects are in proximity to the sensing pad. However, during a touch event due to a finger, the resonance of the sensing antenna decreases to 880 MHz while the resonance of the calibration antenna remains near 940 MHz. The change in return loss due to a touch event should cause the RCS frequency signatures of both tags to change from being nearly identical when no touch event occurs to being distinctly different under a touch event.

To perform the wireless interrogation of the touch sensor, the same Voyantec Tagformance RFID reader is used from the previous section. The reader sends a CW signal at one frequency which is increased in power until the reader is able to read the tag ID from the backscatter. The reader can read multiple tags at once as the EPC-Gen2 protocol has built-in anti-collision mechanisms which allows the reader to determine the RCS of the "sensor" and "calibration" tags at the same time. The RCS measurement is performed at several frequency points to get a frequency-dependent scattering model of both tags to determine the difference in their RCS. Fig. 18(b) shows the measured backscatter results from the touch sensor measurement. It can be seen that under no touch conditions, the RCS of the "sensor" and "calibration"
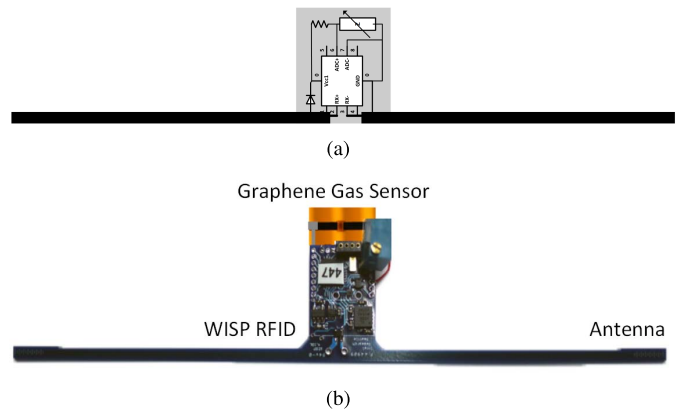

Fig. 19. (a) Design of the WISP-based gas sensor and (b) the WISP-based gas sensor.

tags are nearly identical. This is the expected result from the measured return loss of both tags. When a touch event does occur, the difference in the RCS of both tags increases to approximately 2 dB at some frequencies within the RFID band allowing the reader to determine that there has been a proximity/touch event.

The presented touch sensor demonstrates a simple method to implement wireless touch and proximity sensors at a minimal cost. The sensor is inkjet printed on a paper substrate which allows for ultra-low cost touch sensor implementations which can be integrated into cups for touch and liquid level detection, posters and product stands for wireless user interaction, and a wide array of other interactive applications. Furthermore, by utilizing inkjet-printing, massive quantities of the sensor can be rapidly printed at extremely low-costs [40]–[44].

E. Completely Digital RFID Chip-Based Gas Sensor on a "Universal Wireless Sensing Platform"

A demonstration of the second chip-based sensing topology, in which the sensor data is digitized and modulated along with the chip-ID information into the backscattered signal, is proposed by Le et al. in which wireless sensing of noxious gasses at small ppm levels is performed [6], [45]–[48]. While the previous sensors have all been designed to adapt to
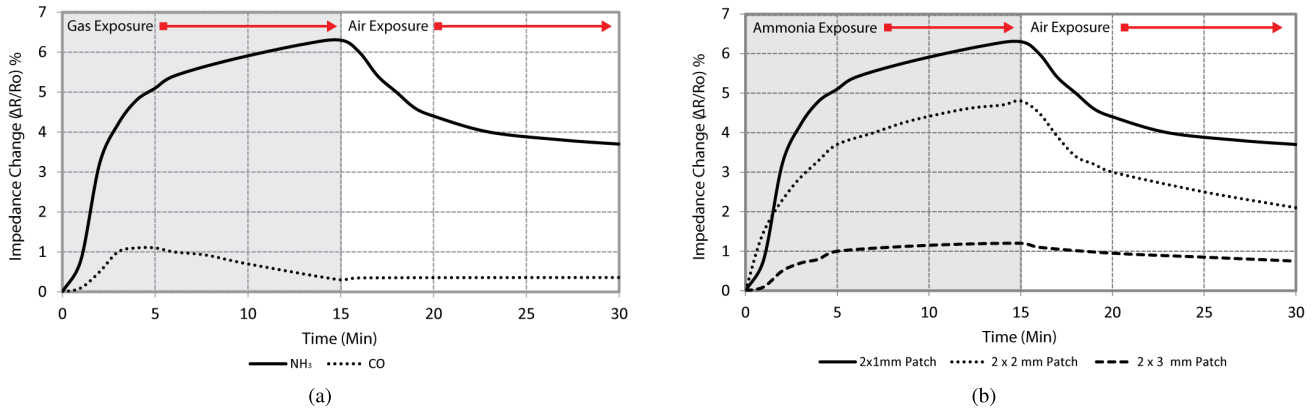
Fig. 20. (a) Measaured senitivity of the graphene gas sensor versus gas flow by the WISP RFID sensing platform and (b) measured sensitivity for three different saturation-point inkjet-printed graphene sensors.

the sensing mechanism, the proposed sensor is based on a "universal" sensing platform which can be adapted to a wide variety of sensors. Gas sensing has become a hot area of interest for household carbon monoxide monitoring, noxious gas monitoring in underground mines and submarines, and ammonia detection as a marker for the early warning of food spoilage. The proposed sensor in Fig. 19(a) is based on the Wireless Identification Sensing Platform (WISP) which is an RFID-compatible sensing platform.

The inkjet-printed graphene-based thin film sensor is highly sensitive to charge transfer by a wide variety of gasses including ammonia, nitrogen oxides, and carbon monoxide. Upon exposure to gas, charge transfer occurs on the high surface area sensor which changes the band structure of the material. This change can be read out as a DC resistance level change. To read this change, the WISP rectifies the incoming RF signal from the interrogator into DC which powers the MCU on the WISP, and supplies a DC voltage to the sensor which is in a resistor divider network. An on-board ADC can then read the voltage across the sensor to determine its resistance value. This value is then digitized and sent in a packet along with the tag ID which can be read by a standard off the shelf RFID reader.

Measurements of the gas sensor to low-ppm exposure to ammonia and carbon monoxide are shown in Fig. 20(a).

The WISP tag is placed inside of a controlled gas chamber, and a level of 10 ppm of each gas is injected into the chamber. An RFID reader is positioned outside of the chamber and continuously reads the data from the RFID tag. The sensitivity curves versus time demonstrate that in less than one minute of low-ppm exposure, the tag can detect resistance changes in the graphene sensor of over 1% for ammonia, and after 5 minutes, changes of up to 5%. There are also different exposure curves for the two different gasses as the charge transfer mechanism for each gas is different. As soon as the gas is turned off, the gas begins to de-adsorb from the graphene surface and the resistance begins to return to its initial value which means the sensor is re-usable.

Several different inkjet printed graphene sensors with different surface areas are then substituted into the resistor divider network in Fig. 19(a) to demonstrate the range of sensitivities obtainable. The results shown in Fig. 20(b) demonstrate that different sensitivities or saturation levels can be obtained utilizing different surface area graphene patches.

The WISP tag is an excellent universal sensing platform as nearly any sensor can be read as long as correct interface circuitry is used. Several other sensors using the WISP platform have already been demonstrated in the literature including strain and temperature sensors [35], [49]. However, because of the high power requirements of the WISP tag, the read range is limited to approximately 3 meters due to FCC limits on transmit power from the reader which is used to power the WISP tag.

F. E-WEHP Autonomous RFID Sensor Platform

The WISP sensing platform demonstrated in the previous section is an excellent "universal" short-range sensing platform which can be adapted to be compatible with a wide range of sensors. However, for long-range sensing where path losses are too high to use backscatter-based interrogation by a reader, the battery-less embedded wireless energy harvesting platform (E-WEHP) has been proposed by Vyas et al. [32]. The foundation of the E-WEHP platform is energy-harvesting based sensing with a system level topology displayed earlier in Fig. 7. On one side, the platform is designed to efficiently harvest energy from ambient RF power. The harvested energy is then used to power a common sensing interface much like the WISP that can digitize and record sensor data. On the other side, there is a transmitter which is used to transmit the sensor data to remote receivers utilizing nearly any RF protocol of choice. This platform essentially switches the energy harvesting mechanism of the WISP platform presented in the previous section from an interrogation signal, to ambient energy sources to allow for much longer range operation.

A listing of typical energy harvesting sources is displayed in Table II. Each energy harvesting source has advantages and limitations that make its usage largely dependent on the environmental conditions and sensor power load requirements.

Ambient/environmental mechanical motion is typically harvested using piezo transducers which are frequency-dependent,

TABLE II
COMPARISON OF AMBIENT ENERGY HARVESTING SOURCES

Energy Source	Average Energy Density
Mechanical	4 uW/cu.cm
Motion	800 uW/cu.cm
Thermal	60 uW/sq.cm
AmbientWireless	1 uW/sq.cm
Solar (Outdoors)	100 mW/sq.cm
Solar (Indoors)	100 uW/sq.cm
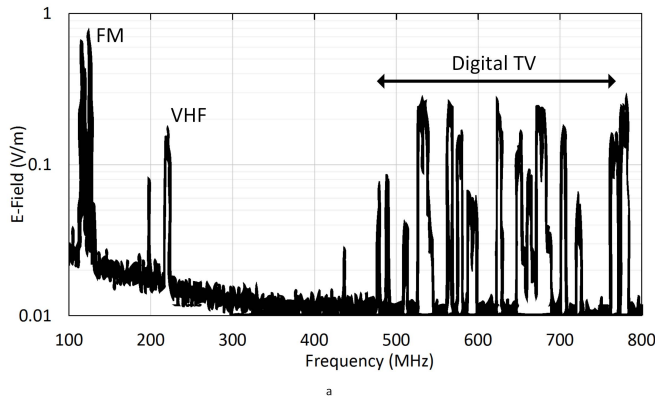
Fig. 21. Measured wireless spectrum in Tokyo, Japan.

Fig. 22. Measured wireless spectrum due to a residential kitchen microwave oven.

Fig. 23. E-WEHP energy harvesting platform.

and typically harvest in to 50–200 Hz range. However, mechanical energy in this frequency range is typically only available on moving objects, or in environments where machinery is operating. Thermal energy harvesting requires high temperature gradients across a thermopile to induce the thermoelectric effect. While this harvesting technique is useful in large grid-server applications where hundred degree gradients are present, standard use areas for sensors do not have high temperature gradients and therefore will not produce useful amounts of energy. Solar is currently the most popular harvesting technique as it works indoors and outdoors as long as there is a line-of-sight light source. Ambient RF power is a relatively new energy harvesting source which gained its popularity from being used to power RFID tags via an RF power-sourcing RFID reader. Even without a power source such as a reader, there are still a wide variety of sources that produce RF energy including TV towers, cellular stations, WiFi routers, and kitchen microwave ovens. Even though mechanical, thermal, and solar energy typically have much higher energy densities than ambient RF energy, ambient is a much more pervasive and constant energy source which can penetrate walls, thin metal, product packaging, and can be harvested from several miles from the energy source.

The average RF energy density in a metropolitan area is displayed in Fig. 21. In this case, the RF snapshot is taken in the middle of the city of Tokyo, Japan. From the spectrum, high energy densities in the FM, and digital TV spectrums are present. While the E-field level of digital TV signal is
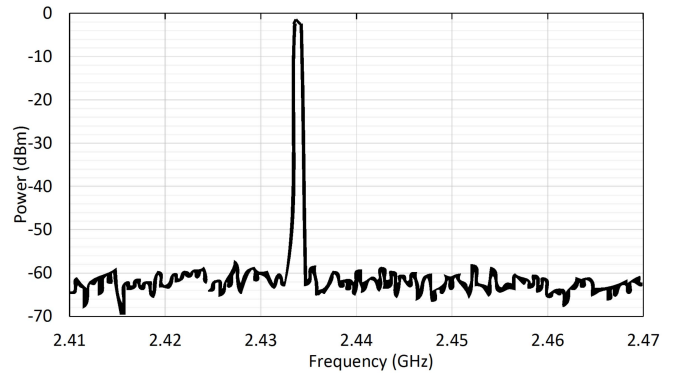
approximately 0.4 V/m which translates to a single tone carrier power of approximately −35 dBm which is not enough a sufficiently high enough energy level to efficiently harvest, the integral of the power over the 500–800 MHz range is approximately −10 to 0 dBm–nearly 1 mW. By exploiting the wideband nature of the digital TV modulation scheme which has a very spectrally efficient broadcast, large amounts of RF energy can be harvested. Furthermore, as current microprocessors can operate in sleep mode at power levels below 50 nW, the ambient RF energy is more than enough to power the microprocessors, ADCs, and low-power transmitters which compose the E-WEHP.

And, while the RF density from TV signals will be lower indoors due to path fading through walls, other sources such as kitchen microwave ovens and WiFi routers emit high levels of RF energy which the E-WEHP system can switch over to. A microwave oven contains a magnetron that produces microwave power of between 500–1000 W in home microwave ovens and 1500–3000 W in commercial microwave ovens. Most magnetrons in microwave ovens emit electromagnetic energy in the 2.45 GHz range.

A spectrum measurement taken several feet away from an operating residential grade microwave oven is displayed in Fig. 22. Power levels as high as 0 dBm, or 1 mW are obtainable. With the addition of WiFi routers, cell phones,
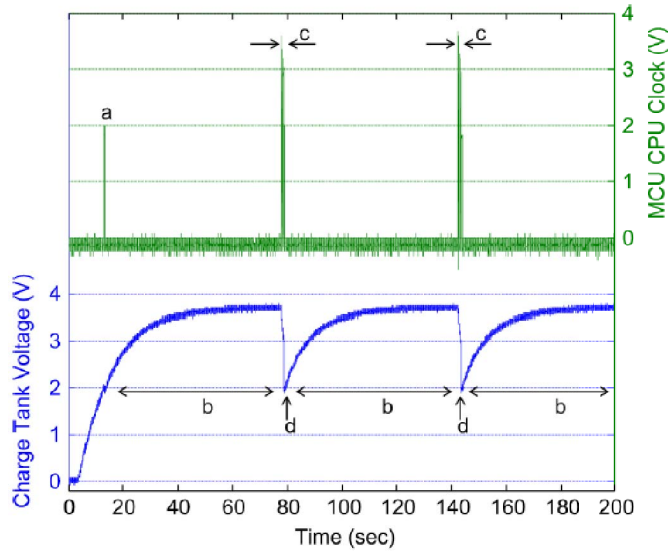
Fig. 24. Oscilloscope capture of the E-WEHP charge tank voltage, and MCU duty cycle while harvesting energy from a TV tower 6.3 away.

and cordless phone systems, several mW can be harvested continuously.

The E-WEHP platform is displayed in Fig. 23. It consists of an RF antenna which can be tuned to capture power in the digital TV (400–800 MHz) band, or microwave oven 2.4 GHz band, a multi-stage charge pump to convert RF to the required DC voltage, a power management unit (PMU) which monitors the energy level stored in the charge tank, a microprocessor (MCU) which reads and stores sensor data, and a transmitter which relays the stored sensor information. Fig. 24 shows the E-WEHP in operation harvesting energy from digital TV signals 6.3 km away from the nearest TV tower and turning on the MCU to perform sensing and communication functions. When the system is first connected, the antenna begins pulling in ambient RF energy and converting it to DC energy which is stored in the charge tank. As the voltage builds up on the charge tank, the PMU monitors the voltage and charging rate to determine when the MCU and transmitter can be turned on, and what period of operation and duty cycle can be sustained at the current RF harvesting rate. Once enough charge is stored in the tank, the MCU wakes from sleep mode and performs the required functions which causes the voltage of the charge tank to drop. Once the voltage reaches a lower threshold, the MCU goes back into sleep mode and the cycle repeats. If the energy being pulled into the system changes due to sensor movement, or a power level change at the source, the E-WEHP detects this change using minimal processing power, and adjusts the duty cycle to compensate.

The E-WEHP is a next-generation autonomous sensor platform which can harvest its own energy and transmit digitized sensor data either indoors, or outdoors at distances of over 6 km from the nearest TV towers. The platform shows promising results for enabling battery-less pervasive and universal wireless RFID sensor networks. The platform can be used for monitoring and increasing cognitive intelligence in disaster areas, populated cities, and urban agricultural environments.

IV. CONCLUSION

Various "zero-power" RFID-based wireless sensing topologies have been investigated which enable low-cost remote sensing and ambient intelligence without the requirement for batteries or wired connections which were previously constraining the scale up and realistic implementation of cognitive wireless sensor networks. Real-world implementation of RFID-based strain, temperature, water quality, and noxious gas sensors presented in this work demonstrate the feasibility of low-cost wireless autonomous sensors to enable pervasive cognitive networks for Internet of Things, smart skins, structural health monitoring, quality of life, and Machine-to-Machine applications.

REFERENCES

[1] J. Zhou, Y. Gu, P. Fei, W. Mai, Y. Gao, R. Yang, *et al.*, "Flexible piezotronic strain sensor," *Nano Lett.*, vol. 8, no. 9, pp. 3035–3040, Aug. 2008.

[2] X. Yi, T. Wu, Y. Wang, R. T. Leon, M. M. Tentzeris, and G. Lantz, "Passive wireless smart-skin sensor using RFID-based folded patch antennas," *Int. J. Smart Nano Mater.*, vol. 2, no. 1, pp. 22–38, Jan. 2011.

[3] B. Cook, A. Shamim, and M. Tentzeris, "Passive low-cost inkjet-printed smart skin sensor for structural health monitoring," *IET Microw. Antennas Propag.*, vol. 6, no. 14, pp. 1536–1541, Nov. 2012.

[4] T. T. Thai, H. Aubert, P. Pons, M. M. Tentzeris, and R. Plana, "Design of a highly sensitive wireless passive RF strain transducer," in *Proc. IEEE MTT-S Int. Symp.*, Jun. 2011, pp. 1–4.

[5] E. Abad, S. Zampolli, S. Marco, A. Scorzoni, B. Mazzolai, A. Juarros, *et al.*, "Flexible tag microlab development: Gas sensors integration in RFID flexible tags for food logistic," *Sens. Actuators B, Chem.*, vol. 127, no. 1, pp. 2–7, Oct. 2007.

[6] L. Yang, R. Zhang, D. Staiculescu, C. Wong, and M. M. Tentzeris, "A novel conformal RFID-enabled module utilizing inkjet-printed antennas and carbon nanotubes for gas-detection applications," *IEEE Antennas Wireless Propag. Lett.*, vol. 8, pp. 653–656, Jul. 2009.

[7] T. Le, V. Lakafosis, S. Kim, B. Cook, M. M. Tentzeris, Z. Lin, *et al.*, "A novel graphene-based inkjet-printed WISP-enabled wireless gas sensor," in *Proc. IEEE 42nd Eur. Microw. Conf.*, Nov. 2012, pp. 412–415.

[8] S. Bouaziz, F. Chebila, A. Traille, P. Pons, H. Aubert, and M. M. Tentzeris, "Novel microfluidic structures for wireless passive temperature telemetry medical systems using radar interrogation techniques in Ka-band," *IEEE Antennas Wireless Propag. Lett.*, vol. 11, pp. 1706–1709, Feb. 2013.

[9] A. Vaz, A. Ubarretxena, I. Zalbide, D. Pardo, H. Solar, A. Garcia-Alonso, *et al.*, "Full passive UHF tag with a temperature sensor suitable for human body temperature monitoring," *IEEE Trans. Circuits Syst. II, Exp. Briefs*, vol. 57, no. 2, pp. 95–99, Feb. 2010.

[10] K. Chang, Y.-H. Kim, Y.-J. Kim, and Y. J. Yoon, "Functional antenna integrated with relative humidity sensor using synthesised polyimide for passive RFID sensing," *Electron. Lett.*, vol. 43, no. 5, pp. 7–8, Mar. 2007.

[11] A. Mainwaring, D. Culler, J. Polastre, R. Szewczyk, and J. Anderson, "Wireless sensor networks for habitat monitoring," in *Proc. 1st ACM Int. Workshop Wireless Sensor Netw. Appl.*, Sep. 2002, pp. 88–97.

[12] M. Cardei and D.-Z. Du, "Improving wireless sensor network lifetime through power aware organization," *Wireless Netw.*, vol. 11, no. 3, pp. 333–340, May 2005.

[13] J. Landt, "The history of RFID," *IEEE Potentials*, vol. 24, no. 4, pp. 8–11, Nov. 2005.

[14] S. Shrestha, M. Balachandran, M. Argarwal, L. Zou, and K. Varahramyan, "A method to measure radar cross section parameters of antennas," *IEEE Trans. Antennas Propag.*, vol. 56, no. 11, pp. 3494–3500, Nov. 2008.

[15] W. T. Wang, Y. Liu, S. Gong, Y. Zhang, and X. Wang, "Calculation of antenna mode scattering based on method of moments," in *Proc. Progr. Electromagn. Res. Lett.*, vol. 15. 2010, pp. 117–126.

[16] A. Bletsas, A. G. Dimitriou, and J. N. Sahalos, "Improving backscatter radio tag efficiency," *IEEE Trans. Microw. Theory Tech.*, vol. 58, no. 6, pp. 1502–1509, Jun. 2010.

[17] I. V. Komarov and S. M. Smolskiy, *Fundamentals of Short-Range FM Radar*. Norwood, MA, USA: Artech House, 2003.

[18] M. Jankiraman, *Design of Multi-Frequency CW Radars*. West Perth, Australia: SciTech, 2007.

[19] S. Preradovic and N. Karmakar, "Multiresonator based chipless RFID tag and dedicated RFID reader," in *Proc. IEEE MTT-S Int. Microw. Symp. Dig.*, May 2010, pp. 1520–1523.

[20] B. S. Cook, A. Shamim, and M. M. Tentzeris, "A passive low-cost inkjet-printed smart skin sensor for structural health monitoring," *IET Microw. Antennas Propag.*, vol. 6, no. 14, pp. 1536–1541, Nov. 2012.

[21] U. Tata, H. Huang, R. L. Carter, and J. C. Chiao, "Exploiting a patch antenna for strain measurements," *Meas. Sci. Technol.*, vol. 20, no. 1, pp. 015201-1–015201-7, Jan. 2009.

[22] S. M. Presas, "Microwave frequency doubler integrated with miniaturized planar antennas," Ph.D. dissertation, Dept. Electr. Eng., Univ. South Florida, Tampa, FL, USA, 2008.

[23] X. Yi, B. S. Cook, C. Cho, J. Cooper, Y. Wang, and M. M. Tentzeris, "Passive frequency doubling antenna sensor for wireless strain sensing applications," in *Proc. ASME Conf. Smart Mater., Adapt. Struct. Intell. Syst.*, Sep. 2012, pp. 625–632.

[24] H. Aubert, F. Chebila, M. Jatlaui, T. Thai, H. Hallil, A. Traille, *et al.*, "Wireless sensing and identification of passive electromagnetic sensors based on millimetre-wave FMCW RADAR," in *Proc. IEEE Int. Conf. RFID-TA*, Nov. 2012, pp. 398–403.

[25] Y. Zhang, L. T. Yang, and J. Chen, *RFID and Sensor Networks: Architectures, Protocols, Security, and Integrations*. Boca Raton, FL, USA: CRC Press, 2010.

[26] U. Karthaus and M. Fischer, "Fully integrated passive UHF RFID transponder IC with 16.7-μw minimum RF input power," *IEEE J. Solid-State Circuits*, vol. 38, no. 10, pp. 1602–1608, Oct. 2003.

[27] P. V. Nikitin and K. Rao, "Performance limitations of passive UHF RFID systems," in *Proc. IEEE Antennas Propag. Soc. Int. Symp.*, Jul. 2006, pp. 1011–1014.

[28] I. Kwon, Y. Eo, H. Bang, K. Choi, S. Jeon, S. Jung, *et al.*, "A single-chip CMOS transceiver for UHF mobile RFID reader," *IEEE J. Solid-State Circuits*, vol. 43, no. 3, pp. 729–738, Mar. 2008.

[29] B. S. Cook, J. R. Cooper, S. Kim, and M. M. Tentzeris, "A novel inkjet-printed passive microfluidic RFID-based sensing platform," in *Proc. Int. Microw. Symp.*, 2013, pp. 1–3.

[30] D. Pardo, A. Vaz, S. Gil, J. Gómez, A. Ubarretxena, D. Puente, *et al.*, "Design criteria for full passive long range UHF RFID sensor for human body temperature monitoring," in *Proc. IEEE Int. Conf. RFID*, Mar. 2007, pp. 141–148.

[31] S. Kim, Y. Kawahara, A. Georgiadis, A. Collado, and M. M. Tentzeris, "Low-cost inkjet-printed fully passive RFID tags using metamaterial-inspired antennas for capacitive sensing applications," in *Proc. Int. Microw. Symp.*, 2013, pp. 2–7.

[32] R. Vyas, B. S. Cook, Y. Kawahara, and M. M. Tentzeris, "E-WEHP: A batteryless embedded sensor-platform wirelessly powered from ambient digital-TV signals," *IEEE Trans. Microw. Theory Tech.*, vol. 61, no. 6, pp. 2491–2505, Jun. 2013.

[33] A. Sample and J. Smith, "Experimental results with two wireless power transfer systems," in *Proc. IEEE RWS*, Jan. 2009, pp. 16–18.

[34] A. Dolgov, R. Zane, and Z. Popovic, "Power management system for online low power RF energy harvesting optimization," *IEEE Trans. Circuits Syst.*, vol. 57, no. 7, pp. 1802–1811, Jul. 2010.

[35] F. Gasco, P. Feraboli, J. Braun, J. Smith, P. Stickler, and L. DeOto, "Wireless strain measurement for structural testing and health monitoring of carbon fiber composites," *Compos., Part A, Appl. Sci. Manuf.*, vol. 42, no. 9, pp. 1263–1274, Sep. 2011.

[36] X. Yi, J. Cooper, V. Lakafosis, R. Vyas, Y. Wang, R. Leon, *et al.*, "Wireless strain and crack sensing using a folded patch antenna," in *Proc. 6th EUCAP*, Mar. 2012, pp. 1678–1681.

[37] X. Yi, C. Cho, B. S. Cook, Y. Wang, M. M. Tentzeris, and R. T. Leon, "Design and simulation of a slotted patch antenna sensor for wireless strain sensing," *Proc. SPIE*, vol. 8694, pp. 1–9, Apr. 2013.

[38] S. Scott and D. Peroulis, "A capacitively-loaded MEMS slot element for wireless temperature sensing of up to 300 C," in *Proc. IEEE MTT-S Int. Microw. Symp. Dig.*, Jan. 2009, pp. 1161–1164.

[39] B. Cook, J. Cooper, and M. Tentzeris, "An inkjet-printed microfluidic RFID-enabled platform for wireless lab-on-chip applications," *IEEE Trans. Microw. Theory Tech.*, vol. 61, no. 12, pp. 4714–4723, Dec. 2013.

[40] B. S. Cook and A. Shamim, "Inkjet printing of novel wideband and high gain antennas on low-cost paper substrate," *IEEE Trans. Antennas Propag.*, vol. 60, no. 9, pp. 4148–4156, Sep. 2012.

[41] B. S. Cook, Y. Fang, S. Kim, T. Le, W. B. Goodwin, K. H. Sandhage, *et al.*, "Inkjet catalyst printing and electroless copper deposition for low-cost patterned microwave passive devices on paper," *Electron. Mater. Lett.*, vol. 9, no. 5, pp. 669–676, Sep. 2013.

[42] B. S. Cook, J. R. Cooper, and M. M. Tentzeris, "Multi-layer RF capacitors on flexible substrates utilizing inkjet printed dielectric polymers," *IEEE Microw. Compon. Lett.*, vol. 23, no. 7, pp. 353–355, Jul. 2013.

[43] B. Cook, B. Tehrani, J. Cooper, and M. Tentzeris, "Multilayer inkjet printing of millimeter-wave proximity-fed patch arrays on flexible substrates," *IEEE Antennas Wireless Propag. Lett.*, vol. 12, pp. 1351–1354, Oct. 2013.

[44] L. Yang, A. Rida, R. Vyas, and M. M. Tentzeris, "Rfid tag and RF structures on a paper substrate using inkjet-printing technology," *IEEE Trans. Microw. Theory Tech.*, vol. 55, no. 12, pp. 2894–2901, Dec. 2007.

[45] T. Le, V. Lakafosis, Z. Lin, C. P. Wong, and M. M. Tentzeris, "Inkjet-printed graphene-based wireless gas sensor modules," in *Proc. IEEE 62nd ECTC Conf.*, Jun. 2012, pp. 1003–1008.

[46] T. Le, V. Lakafosis, S. Kim, B. S. Cook, M. M. Tentzeris, Z. Lin, *et al.*, "A novel graphene-based inkjet-printed WISP-enabled wireless gas sensor," in *Proc. 42nd Eur. Microw. Conf.*, Nov. 2012, pp. 412–415.

[47] L. Yang, A. Rida, and M. M. Tentzeris, "Design and development of radio frequency identification (RFID) and RFID-enabled sensors on flexible low cost substrates," *Synth. Lect. RF/Microw.*, vol. 1, no. 1, pp. 1–89, Jan. 2009.

[48] R. Vyas, V. Lakafosis, H. Lee, G. Shaker, L. Yang, G. Orecchini, *et al.*, "Inkjet printed, self powered, wireless sensors for environmental, gas, and authentication-based sensing," *IEEE Sensors J.*, vol. 11, no. 12, pp. 3139–3152, Dec. 2011.

[49] S. A. Ahson and M. Ilyas, *RFID Handbook: Applications, Technology, Security, and Privacy*. Boca Raton, FL, USA: CRC Press, 2010.

Benjamin S. Cook, photograph and biography not available at the time of publication.

Rushi Vyas, photograph and biography not available at the time of publication.

Sangkil Kim, photograph and biography not available at the time of publication.

Trang Thai, photograph and biography not available at the time of publication.

Taoran Le, photograph and biography not available at the time of publication.

Anya Traille, photograph and biography not available at the time of publication.

Herve Aubert, photograph and biography not available at the time of publication.

Manos M. Tentzeris, photograph and biography not available at the time of publication.